

Optical properties of the NGC 5328 group of galaxies^{*}

R. Grützbauch¹, F. Annibali², A. Bressan^{2,3}, P. Focardi⁴, B. Kelm⁴,
 R. Rampazzo³, W.W. Zeilinger¹

¹ Institut für Astronomie, Universität Wien, Türkenschanzstraße 17, A-1180 Wien, Austria

² SISSA, via Beirut 4, I-34014 Trieste, Italy

³ INAF - Osservatorio Astronomico di Padova, Vicolo dell'Osservatorio 5, I-35122 Padova, Italy

⁴ Dipartimento di Astronomia, Università di Bologna, Via Berti Pichat 6, I-40127 Bologna, Italy

Accepted. Received; in original form

ABSTRACT

We present the results of a photometric and spectroscopic study of seven members of the NGC 5328 group of galaxies, a chain of galaxies spanning over 200 kpc ($H_0=70$ km s⁻¹Mpc⁻¹). We analyze the galaxy structure and study the emission line properties of the group members looking for signatures of star formation and AGN activity. We finally attempt to infer, from the modeling of line-strength indices, the stellar population ages of the early-type members. We investigate also the presence of a dwarf galaxy population associated with the bright members.

The group is composed of a large fraction of early-type galaxies including NGC 5328 and NGC 5330 two “bona fide” ellipticals at the center of the group. In both galaxies no recent star formation episodes are detected by the H β vs. MgFe line-strength indices of these galaxies. 2MASX J13524838-2829584 has extremely boxy isophotes which are believed to be connected to a merging event: line strength indices suggest that this object probably had a recent star formation episode. A warped disc component emerges from the model subtracted image of 2MASX J13530016-2827061 which is interpreted as a signature of an ongoing interaction with the rest of the group.

Ongoing star formation and nuclear activity is present in the projected outskirts of the group. The two early-type galaxies 2MASX J13523852-2830444 and 2MASX J13525393-2831421 show spectral signatures of star formation while a Seyfert 2 type nuclear activity is detected in MCG -5-33-29.

Key words: Galaxies: distances and redshifts; Galaxies: photometry; Galaxies: spectroscopy; Galaxies: interactions; Galaxies: groups of galaxies

1 INTRODUCTION

Recent investigations tend to map galaxy properties in the cluster outskirts and beyond, at local densities typical of galaxy groups and where a pre-processing of the subsequent cluster galaxies could take place (Lewis et al. 2002; Bower & Balog 2004; Mihos 2004). The dynamically relaxed centers of clusters are surrounded by infall regions in which galaxies are bound to the cluster but not in an equilibrium configuration. The mass of such an infall region could be of the order 20 - 120% of the virial mass, showing that clusters are still forming (Rines et al. 2003). The galaxy population in that region is not pristine, since significant preprocessing in group-like environments are expected (Gill et al. 2005). Groups of galaxies, of different richness and density, are also

typical galaxy aggregates of low density environments. Since they contain a substantial fraction of the mass of the Universe, it is of crucial importance to shed light about the galaxy evolution in such an environments.

The low velocity dispersion in groups leads to slow encounters between member galaxies and is predicted to trigger star formation episodes (see e.g. Kennicutt, Schweizer & Barnes 1996) and AGN activity. Nearby groups do not show, however, firm evidence for galaxy activity enhancement (Verdes-Montenegro et al. 1998; Coziol et al. 2000; Maia et al. 2003; Kelm et al. 2004; Tanvua et al. 2003). The interaction processes are not only altering the overall characteristics of the involved galaxies, they also could affect the group galaxy population (e.g. via galaxy-galaxy merging and/or formation of tidal dwarf galaxies (see e.g. Duc et al. 2004, and references therein) and of the IGM).

Recent X-ray studies have shown that a signifi-

^{*} Based on observations collected at European Southern Observatory, La Silla, Chile (Programme Nr. 65.P-252)

cant amount of a diffuse emission could be present in galaxy groups (Mulchaey et al. 1993, 1996; Ponman et al. 1996; Mulchaey 2000; Mulchaey et al. 2003; Gomez et al. 2003, see e.g.) and even in physical pairs composed of an elliptical and a spiral member (Rampazzo et al. 1998; Henriksen & Cousineau 1999; Trinchieri & Rampazzo 2001). However it is still unclear whether massive groups, whose dominant galaxy is a spiral, do exist (Mulchaey 2000; Kelm & Focardi 2004).

Evolutionary phenomena in poor structures are furthermore of interest in the context of a evolving galaxy groups since candidate “fossil groups”, i.e. the debris of a pristine group, are found at low and intermediate redshifts (Mulchaey & Zabludoff 1999; Jones et al. 2003). The evolutionary scenario of isolated galaxy groups raises then fundamental questions: what is the final stage of small galaxy structures in the field? Are they stable and long-lived structures or does their evolution lead to the formation of giant elliptical galaxies in the field traced by the detected X-ray diffuse emission?

Several arguments indicate that photometric parameters of massive ellipticals are not compatible with their formation being the result of several major merging events diluted along the Hubble time (Meza et al. 2003). Moreover, massive early-type galaxies in low density environments appear on the average only 2 Gyr younger than their counterparts in high density environments (Thomas et al. 2005). Because a considerable fraction of massive galaxy formation in low density environments occurs at redshifts $1 < z < 2$, the end product of groups observed out to $z \approx 1$ could not easily be a new massive early-type galaxy.

In this paper we present the optical, photometric and spectroscopic properties of the poor group dominated by the bright elliptical galaxy NGC 5328. The group has a compact and elongated shape: galaxies are basically aligned in a long chain spanning from Northeast to Southwest. NGC 5328 is well centered within this galaxy chain. This group is located in the vicinity of the Abell 3574 cluster of galaxies. Our photometric and spectroscopic investigation covers the central part of the group including seven spectroscopically confirmed, bright member galaxies distributed over a radius of about 100 kpc ($H_0=70 \text{ km s}^{-1} \text{ Mpc}^{-1}$). We also provide positions and the basic photometric properties of dwarf galaxies, lying within our frames, candidate members of the group.

The paper is organized as follows. In Section 2 we summarize the literature data about NGC 5328 group. Section 3 presents the observations and the data reduction. The detailed surface photometry, the analysis of galaxy structures and a preliminary description of the spectroscopic properties of each galaxy are given in Section 4. Medium-resolution spectroscopy is used to establish group memberships and to analyze the spectral energy distributions in order to check possible features like induced activity and enhanced star formation. Line-strength indices which, transformed into the Lick-IDS system, were modeled to infer the star formation history of the bright galaxies in the group, are presented in Section 5. The group properties are finally discussed in the context of the literature and in particular of our previous works on this subject (Tanvua et al. 2003, paper I) and Grützbauch et al. (2005, paper II).

2 THE NGC 5328 GROUP IN THE LITERATURE

The NGC 5328 group of galaxies was first mentioned by Klemola (1969) as the object nr. 28 in his catalogue of “Groups and Clusters of Southern Galaxies”. The author described the structure as a “group of round or somewhat elongated galaxies with one spiral to NE”. In the original description, Klemola 28 consists of 7 galaxies within an area of $15' \times 5'$, although the member galaxies are not named. Given the coordinates of Klemola 28 and the description of the group structure, we presume that the members of Klemola 28 coincide with the bright galaxies of the present study.

Garcia (1993) associates NGC 5328 with the well studied Seyfert galaxy IC 4329 and 21 other galaxies to the group LGG 357. A quite similar set of galaxies is given by Giuricin et al. (2000) in his NOG 725. None of the galaxies considered in our study is part of the LGG or the NOG sample. IC 4329 is located at a projected distance of about 2.5 Mpc from NGC 5328 and belongs to the Abell 3574 cluster of galaxies, a poor cluster consisting of 55 spectroscopically confirmed member galaxies moving with a recession velocity of $cz = 4797 \text{ km s}^{-1}$ and having a velocity dispersion of $\sigma = 793 \text{ km s}^{-1}$ (Struble & Rood 1999). In the red-shift space our group and the cluster form a coherent structure with a virtually null difference in their systemic velocity ($v_{\text{cluster}} - v_{\text{NGC 5328}} = 39 \text{ km s}^{-1}$). The projected separation between the NGC 5328 group and the cluster outskirts amounts to $\approx 1^{\circ}20'$ (corresponding to 1.7 Mpc). Thus, although the group cannot be characterized as a substructure of the cluster, the group and the cluster could be potentially connected. Richter (1984) presents a list of prominent galaxies on the plates 444 and 445 of the ESO-SRC Survey, giving the morphological classifications for all galaxies in our sample and including redshifts for NGC 5328 and NGC 5330.

Concerning the properties of individual galaxies of our sample, MCG -5-33-29 is quoted in the “Catalog of Southern Ringed Galaxies” (Buta 1995) but only NGC 5328 has been studied in detail so far. de Carvalho & da Costa (1988) presented a detailed surface photometry, indicating that NGC 5328 is a “bona fide” elliptical. Several values for the central velocity dispersion are available, with an average of 303 km s^{-1} (<http://www-obs.univ-lyon1.fr/hypercat>), the latest measurement by Smith et al. (2000) amounts to $\sigma = 314 \pm 7 \text{ km s}^{-1}$ suggesting that it is a massive galaxy. NGC 5328 is a relatively strong X-ray emitter. Beuing et al. (1999) report a value of $\log L_X = 42.03 \pm 0.072 \text{ erg s}^{-1}$ within a radius of $16.25'$. The morphology and the characteristics of the X-ray emission are not discussed. Mahdavi & Geller (2001) presented a unified relation between L_X and σ for 280 clusters and 57 galaxies of the form $L_X \propto \sigma^m$ with a slope steepening from $m=4.4$ for clusters to $m=10.2$ for individual galaxies. The relation for groups is not that well defined and shows a larger scatter suggesting that most of them have either not yet reached dynamical equilibrium or the emission is produced by unresolved sources in the IGM. NGC 5328 is included in the sample of individual galaxies and lies exactly on the $L_X \propto \sigma^{10.2}$ relation. The discussion of the X-ray properties of NGC 5328 as a group, and its evolutionary phase, then awaits more detailed X-ray observations.

Table 1. Observing log of imaging

(1)	(2)	(3)	(4)	(5)	(6)	(7)
1	13 ^h 52 ^m 54 ^s	-28°29'05"	4×60	1.10	2×300	1.05
2	13 ^h 52 ^m 47 ^s	-28°31'36"	3×30	1.00	3×300	0.96
3	13 ^h 53 ^m 09 ^s	-28°27'18"	3×60	1.13	3×300	1.08

¹ field nr.; ² α (J2000.0); ³ δ (J2000.0); ⁴ R-band exposure time [s]; ⁵ R-band seeing FWHM [arcsec]; ⁶ B-band exposure time [s]; ⁷ B-band seeing FWHM [arcsec].

3 OBSERVATIONS AND DATA REDUCTION

The observations were performed at the ESO 3.6m telescope in La Silla, Chile during the nights of 5th and 6th May 2000. Details of the observations and the data reduction procedures are therefore described in paper II.

In order to cover the central part of the NGC 5328 group a mosaic of 3 images has been assembled. The observing log of imaging containing the field coordinates, exposure time and seeing conditions is given in Table 1. Long-slit medium-resolution spectra have been obtained for 8 galaxies to obtain the spectral information of the candidate member galaxies. Table 2 shows the instrumental set-up of the spectroscopic observations. The velocity dispersion values given in Table 3 were determined by performing Gaussian fits to single spectral lines. The FWHM of the fitted profiles were corrected for the instrumental dispersion, but the large instrumental dispersion of $\sigma_{inst} = 227 \text{ km s}^{-1}$ biases the measurements toward higher values. The values of σ in Table 3 can therefore only give a rough estimate of the galaxies' true velocity dispersion.

The mosaic image of the group shown in Figure 1 covers $\approx 60 \text{ arcmin}^2$. The seven spectroscopically confirmed member galaxies listed in Table 3 are indicated in the figure. The group structure has an elongated shape, six of seven member galaxies are aligned in a chain spanning from the southwest to the northeast. The bright elliptical galaxy NGC 5328 lies roughly in the center of this galaxy chain. The mean projected separation of the seven member galaxies amounts to $\approx 200 \text{ kpc}$.

In order to extend our understanding of the group properties we attempted the detection of candidate dwarf galaxies members of the group in our B and R band exposures. The **SourceExtractor** (Bertin et al. 1996) was used to detect extended sources, i.e. having a *stellaricity* parameter ≤ 0.5 . The candidate sample was limited in magnitude ($m_R \leq 21^{\text{mag}}$) and size ($a \geq 2 \text{ arcsec}$), furthermore, a colour restriction was applied in the attempt to exclude background objects (see e.g. Khosroshahi et al. 2004). The trend with fainter magnitudes toward bluer colours, reflecting the expected lower metallicities of less massive galaxies, is present in our group sample. For our faint galaxy sample, this trend is well defined in the blue colour regime, while on the red side the contamination with background objects becomes visible. A colour restriction of $0.7 \leq (B-R) \leq 1.9$, representing generous limits to the early-type sequence, was found to be likely to remove the vast majority of background objects. The resulting sample of likely dwarf galaxy group members consists of 68 objects with a mean colour of $(B-R) = 1.32 \pm 0.28 \text{ mag}$. The magnitudes and the $(B-R)$ colour of this 68 extended sources are given in the Appendix, Ta-

bles A1 and A2. We did not perform surface photometry on the dwarf galaxy candidates because our observations are not deep enough to provide an accurate surface photometry.

4 RESULTS

The relevant spectroscopic and photometric results about the seven member galaxies of the NGC 5328 group are summarized in Table 3 and Table 4 respectively. We collect in Table 5 the results of a research (done using the NED) about galaxies with known redshift within 1 Mpc from NGC 5328 representing possible members/neighbours of the group. These latter are not uniformly distributed around the group, but are located within two narrow cones perpendicular to the orientation of the chain.

In the sub-sections below we detail the photometric and spectroscopic results.

4.1 Photometric results and individual notes

Surface photometry of the bright group member galaxies has been carried out with the ellipse fitting routine provided by the **STSDAS** package within **IRAF**¹ and with the **GALFIT** package (Peng et al. 2002). While the **ELLIPSE** task computes a Fourier expansion for each successive isophote (Jedrzejewski 1987), **GALFIT** was used to perform a bulge-disc decomposition in the case of early-type galaxies and to determine the parameters of a Sersic model fit to the galaxies bulge component. The Sersic profile is the generalization of the de Vaucouleur's law with $\mu(r) \sim r^{1/n}$, where the Sersic parameter n is a free parameter. This profile is thus sensitive to structural differences between different kinds of early type galaxies and providing a better fit to real galaxy profiles. Only the surface brightness profile of NGC 5328 was fitted by $n \sim 4$, whereas the other objects are featuring a variety of Sersic parameters in the range $1 \leq n \leq 4$.

For each member galaxy the isophotal map, the B-band image and the residual after a model subtraction to reveal fine structure, disc components, spiral arms or other patterns are shown in Figures 2 and 3. The surface photometry profiles including surface brightness, ellipticity, position angle, the coefficients of the Fourier expansion and the $(B-R)$ colour profile are displayed in Figures 4, 5 and 6.

NGC 5328 The surface photometry (Figure 4, top left) shows a $r^{1/4}$ surface brightness profile over a range of 7 mag suggesting that the galaxy is a "bona fide" elliptical. The ellipticity distribution increases in the range of $0.2 < \varepsilon < 0.4$ up to a radius of $7''$ where it becomes flat. The b_4 profile is basically flat although a possible discy structure appears in the residual image in Figure 2 (top row, right panel). We classified NGC 5328 as E3 in contrast to the classification as E1 by de Vaucouleurs et al. (1991). The colour profile is almost flat at a value of $(B-R) \approx 1.7 \text{ mag}$.

NGC 5330 The surface brightness profile of this nearly round elliptical was fitted by a Sersic power law with

¹ **IRAF** is distributed by the National Optical Astronomy Observatories, which are operated by the Association of Universities for Research in Astronomy Inc., under cooperative agreement with the National Science Foundation.

Table 2. Spectroscopic observations

field nr.	exp. t. [s]	sl.-wid. ["]	P.A. [°]	object	wav. range [Å]
1	2×1200	1.0"	132°	NGC 5328	4070 – 7470
				NGC 5330	4070 – 7470
2	2×1200	1.0"	111°	2MASX J13524838-2829584	4070 – 7470
				2MASX J13523852-2830444	4070 – 7470
2	2×1200	1.0"	10°	2MASX J13525552-2834001 (B1)	4070 – 7470
				2MASX J13525393-2831421	4070 – 7470
3	2×1200	1.0"	115°	MCG -5-33-29	4070 – 7470
				2MASX J13530016-2827061	4070 – 7470

Table 3. Spectroscopic Results

object	α (J2000.0)	δ (J2000.0)	type	V_{hel} [km s $^{-1}$]	D 1 [kpc]	σ_0 [km s $^{-1}$]	id. Fig.1
NGC 5328	13 h 52 m 53.6 s	-28°29'16"	E3	4785 \pm 131	–	303 2	1
NGC 5330	13 h 52 m 59.2 s	-28°28'15"	E1	4737 \pm 60	35	292 \pm 60	2
2MASX J13524838-2829584	13 h 52 m 48.4 s	-28°29'58"	S0	4566 \pm 76	26	246 \pm 118	3
2MASX J13523852-2830444	13 h 52 m 38.5 s	-28°30'45"	S0	5452 \pm 43	63	–	4
2MASX J13525393-2831421	13 h 52 m 53.9 s	-28°31'42"	SB0	5153 \pm 51	47	–	5
2MASX J13530016-2827061	13 h 53 m 00.2 s	-28°27'06"	S0	5243 \pm 90	57	298 \pm 127	6
MCG -5-33-29	13 h 53 m 15.6 s	-28°25'33"	SB(r)a	4625 \pm 164	124	–	7

1 Projected distance from NGC 5328 ($H_0 = 70 \text{ km s}^{-1} \text{Mpc}^{-1}$); 2 The value of the velocity dispersion quoted for NGC 5328 is taken from Rampazzo et al. (2005) since it has been used for the calibration of line-strength indices to the Lick-IDS systems.

a high structural parameter of $n = 3.16$, with the isophotes showing no deviations from pure ellipses (see Figure 4, top right). The average ellipticity is ≈ 0.1 , while the position angle variation outside the region affected by the seeing is less than 10° . Like 2MASX J13524838-2829584, NGC 5330 is embedded in the outer halo of NGC 5328 from which it is separated by 35 kpc in projection. The luminosity and geometric profiles of NGC 5330 are contaminated by the light of the nearby giant elliptical. The contamination is probably the cause for the observed increase of the (B-R) colour profile at radii $r > 16''$. The model subtracted image shows a faint ripple-like residual at $r \approx 10''$ which does not seem to be an artifact since the isophotes in that region – as shown in Figure 4 – are nearly perfect ellipses and show virtually null variation of their position angle.

MCG -5-33-29 The SBa spiral is located at about 124 kpc projected distance from NGC 5328. The arms start from a bar at $r \approx 10''$ and appear tightly wound. The bar can be seen in the flattening of the surface brightness profile at $r \approx 11''$. The (B-R) colour profile in the bar region is flat and red (≈ 1.75 mag) and drops to ≈ 1.4 mag in the position of the arms and the ring. The model subtracted image (Figure 3) reveals the irregular patchy structure of the spiral arms which both appear bifurcated.

2MASX J13524838-2829584 The surface photometry of this small galaxy is strongly contaminated by the vicinity of NGC 5328. The inner parts are slightly discy while the outskirts are quite boxy ($b_4 = -0.05$). The position angle variation of about 10° is only marginally due to the light contamination caused by NGC 5328. The colour profile is red and flat at (B-R)=1.65.

2MASX J13523852-2830444 The morphology sug-

gests a S0-type galaxy seen almost edge-on. The presence of a disc is supported by the increasing ellipticity $0.2 \leq \varepsilon \leq 0.6$ and the constant position angle profiles with a variation lower than 5° . The results from the surface photometry are affected by a central major-axis dust lane, whose signature is evident in the residual image (Figure 2) and in the positivity of the b_4 parameter.

2MASX J13525393-2831421 We classify this galaxy as an SB0. This classification is based upon the surface brightness profile showing two components and the sudden isophotal twisting of about 20° , indicating the presence of a bar component as suggested also in the isophotal image of Figure 3. The (B-R) colour profile has an average value of 1.5 mag.

2MASX J13530016-2827061 This galaxy is an edge-on S0 galaxy with a weak disc component, merely distinguishable in the surface brightness profile, but clearly visible in ellipticity, position angle and the b_4 profile. The residual image in Figure 3 shows the typical pattern of positive 4th Fourier-coefficients indicative of strong discy isophotes. The disc is thickening with increasing radius and is warped in its outer parts.

4.2 Spectroscopic results

Table 3 collects the relevant information coming from the spectroscopic study of the NGC 5328 group members. Figure 7 shows the spectra obtained from seven member galaxies. Both NGC 5328 and NGC 5330 show absorption-line spectra typical of elliptical galaxies. The spectra of 2MASX J13524838-2829584 and 2MASX J13530016-2827061 are consistent with their class and do not show peculiarities.

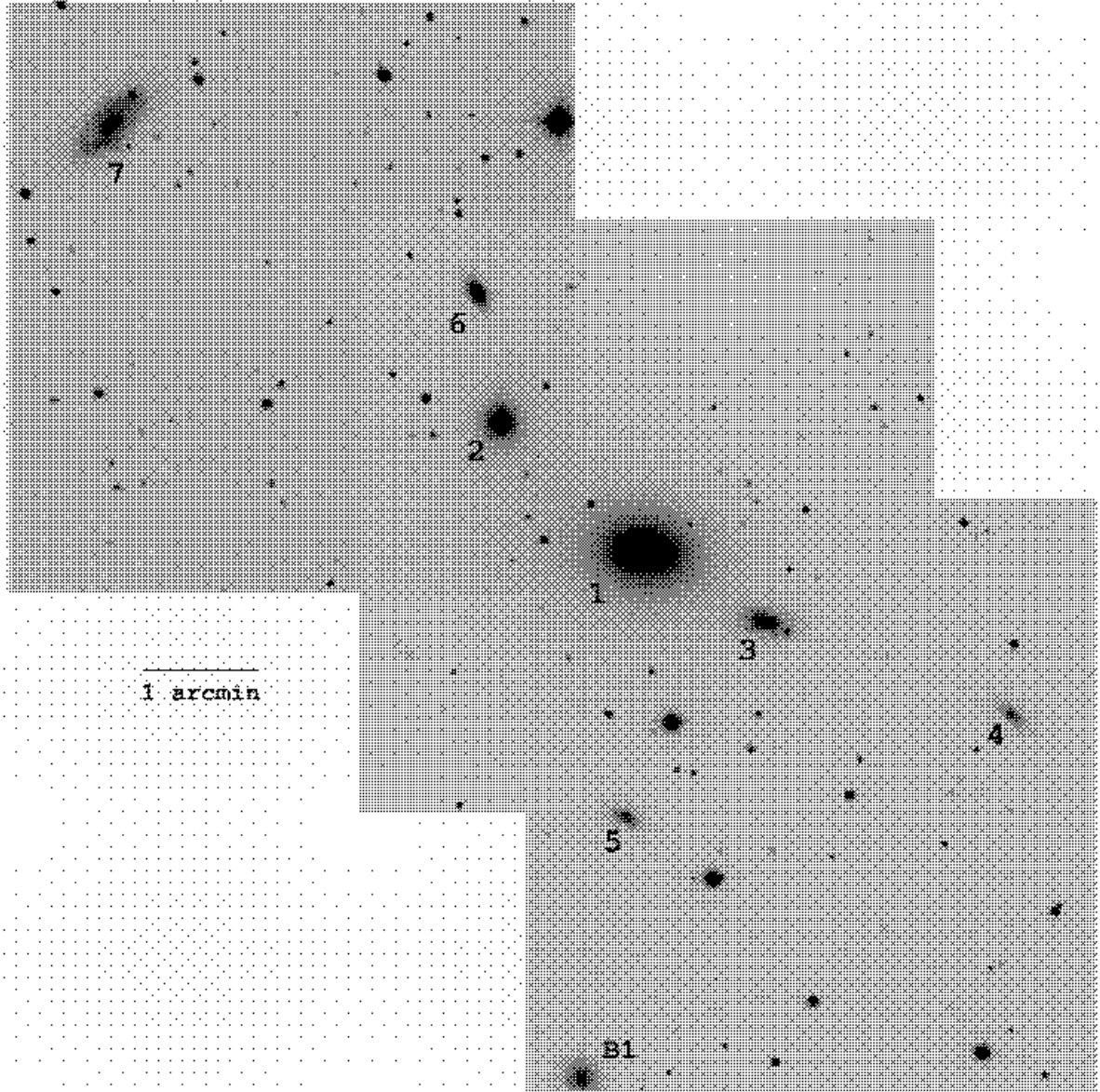


Figure 1. B-band mosaic image of the NGC 5328 group of galaxies. The group members are numbered accordant to Table 3. The redshift of the galaxy labelled B1 has been measured and is not concordant with that of the group.

Emission lines are shown by the remaining three galaxies. The spectrum of the spiral MCG -5-33-29 presents narrow but strong forbidden lines of [O III], [N II] and [S II]. H α is weak in emission and H β is weak in absorption. Figure 7 shows the emission features in 2MASX J13523852-2830444 in the region around H α featuring narrow emission lines of H α , [N II] and [S II]. 2MASX J13525393-2831421 shows strong H α emission and only weak [N II] and [S II] lines.

The average recession velocity of the group is 4937 (median 4785) km s $^{-1}$ with a velocity dispersion of $\sigma = 342$ km s $^{-1}$, while in the projected innermost part of the group, which includes NGC 5328, NGC 5330 and 2MASX J13530016-2827061, the dispersion is significantly lower (279 km s $^{-1}$). The virial mass of the group based on our redshift measurements and the projected separa-

tions between each galaxy pair has been computed according to Heisler, Tremaine & Bahcall (1985). Although it is susceptible to systematic errors due to the incompleteness of the sample, the probable non-equilibrium state of the group or projection effects, it still represents a straightforward and common mass estimator for galaxy groups. Inclusion of galaxies lying within 1 Mpc from NGC 5328 (see 5) yielded $M_{VT} = 1.6 \times 10^{13} M_{\odot}$, which is a typical value for poor galaxy groups.

4.3 Properties of emission lines and absorption line-strength indices

The properties of the detected emission lines were used to characterize and classify the group members. Emission line EWs have been measured by modeling the underlying stel-

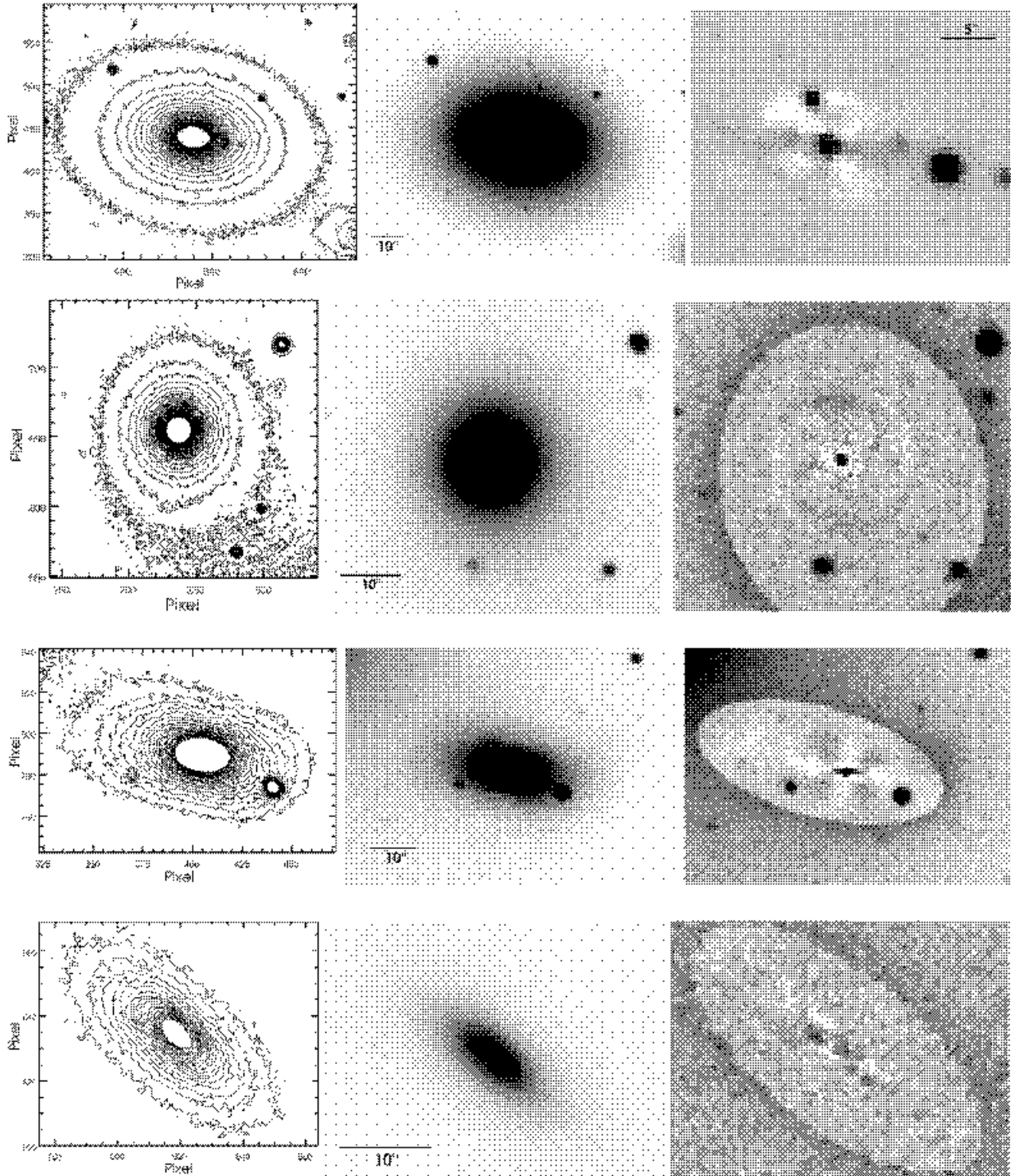


Figure 2. Analysis of fine structure in galaxies: isophote structure (left panels), original image (mid panels) and model subtracted images (right panels). From top to bottom: NGC 5328, NGC 5330, 2MASX J13524838-2829584 and 2MASX J13523852-2830444.

lar component and subtracting it to each galaxy spectrum (see also next paragraphs). The derived emission-line ratios are plotted in the diagnostic diagrams proposed by Veilleux & Osterbrock (1987) shown in Figure 8. According to these diagrams, the spiral MCG -5-33-29 has emission properties typical of an AGN while both the S0s 2MASX

J13523852-2830444 and 2MASX J13525393-2831421 present emissions features characteristic of HII regions, suggesting the presence of ongoing or recent star formation in their centers.

Recently Rampazzo et al. (2005) presented a study of line-strength indices calibrated in the Lick-IDS system

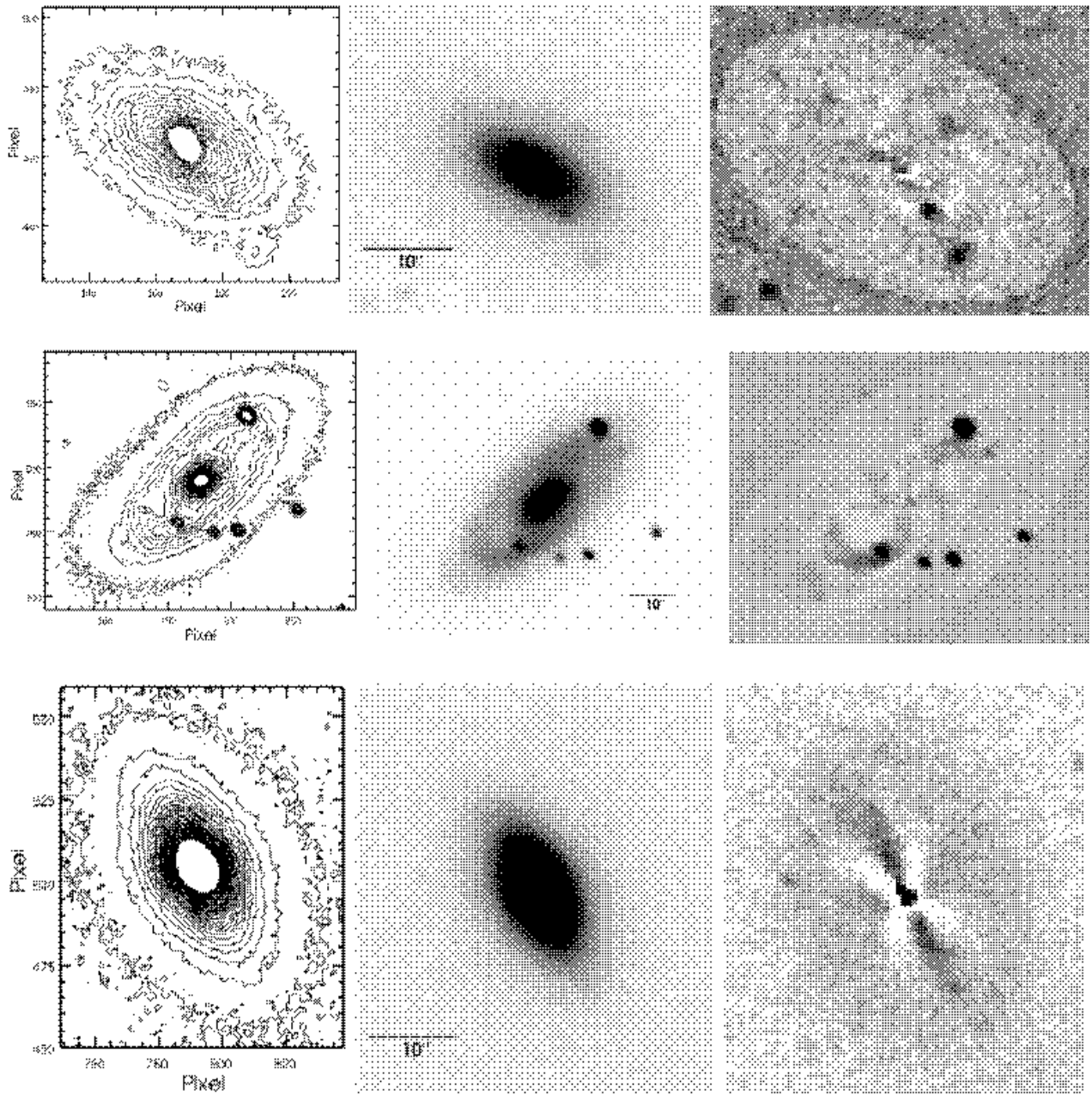


Figure 3. Analysis of fine structure in galaxies: isophote structure (left panels), original image (mid panels) and model subtracted images (right panels). From top to bottom: 2MASX J13525393-2831421, MCG -5-33-29 and 2MASX J13530016-2827061.

(Worley & Ottaviani 1997) for a sample of early-type galaxies which also includes NGC 5328. Using the spectrum of NGC 5238 as reference, the same calibration procedure was applied to remaining galaxy spectra of the group as described in (Rampazzo et al. 2005). The full procedure includes the correction for possible hydrogen emission, correction for velocity dispersion and the transformation to the Lick-IDS system. We are aware that the standard calibration to the Lick system lies on the observation and the comparison with a set of Lick-IDS standard stars. For this transformation Lick-IDS standard stars have been observed but yielded unsatisfactory calibration results. We then approached the transformation to the Lick-system by compar-

ing our raw indices of NGC 5328, measured for 7 different apertures, with the corresponding corrected line-strength indices for the same galaxy obtained by Rampazzo et al. (2005). The comparison is shown in Figure 9. In the literature (see also Puzia et al. 2002) the transformation to the Lick system is computed by fitting the points with a linear relation of the kind $EW_{Lick} = \alpha EW_{raw} + \beta$. For most of the indices the slopes of the transformation are very close to 1 and only a zero point offsets are required. Given the limited number of points, the small variation of each index, and the "non standard" procedure, we calculated the correction to the Lick system forcing $\alpha=1$ in the fit and deriving only the offsets β . In Figure 9 the dotted line is the one to

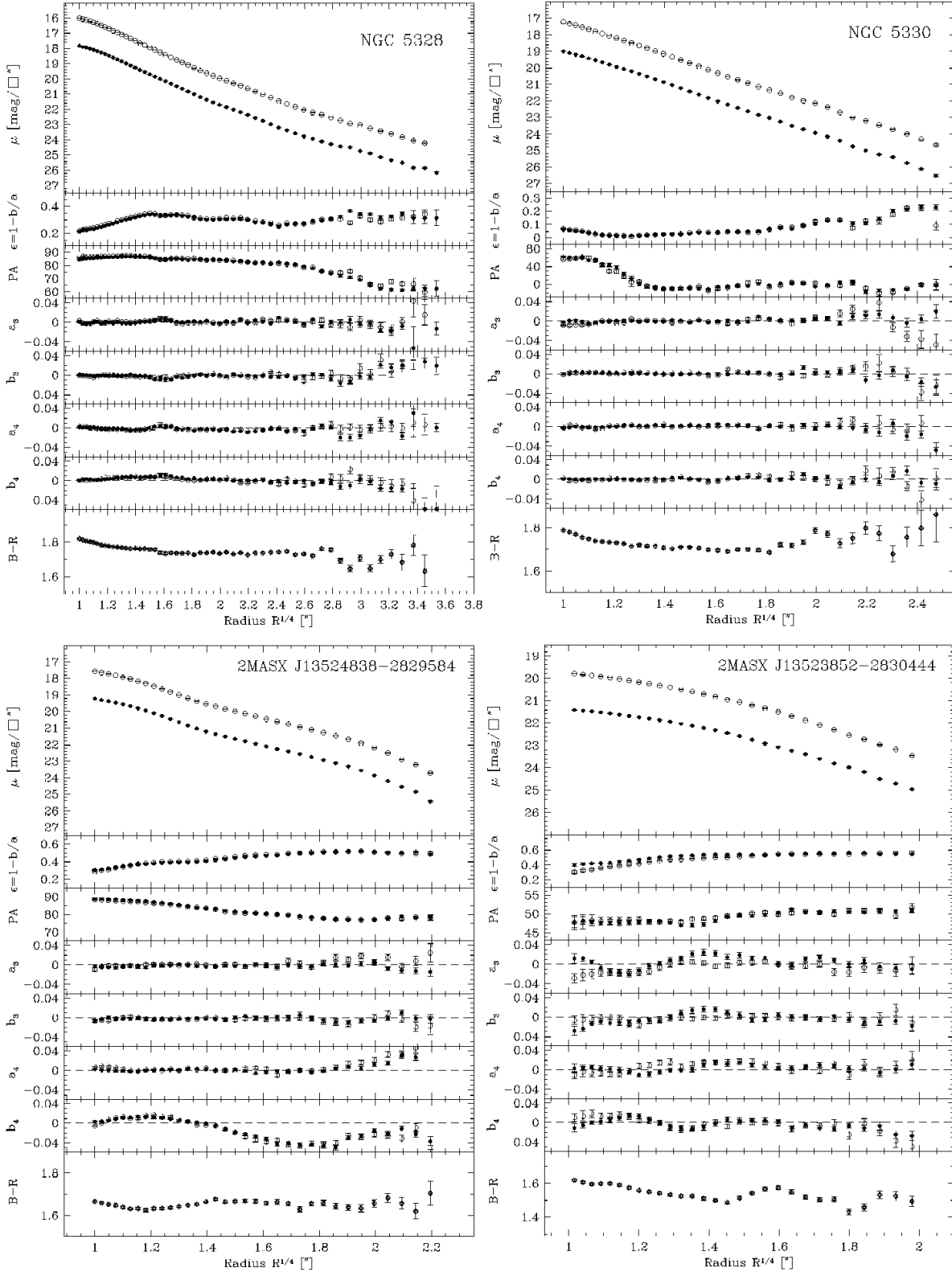


Figure 4. B (full circles) and R (open circles) bands surface photometry of group member galaxies. From top to bottom: surface brightness (μ), ellipticity (ϵ), position angle profile (P.A.), higher order coefficients of the Fourier expansion from the interpolation of isophotes with ellipses (a_3 , b_3 , a_4 , b_4) and (B-R) colour profiles. In particular b_4 is the isophotal shape parameter.

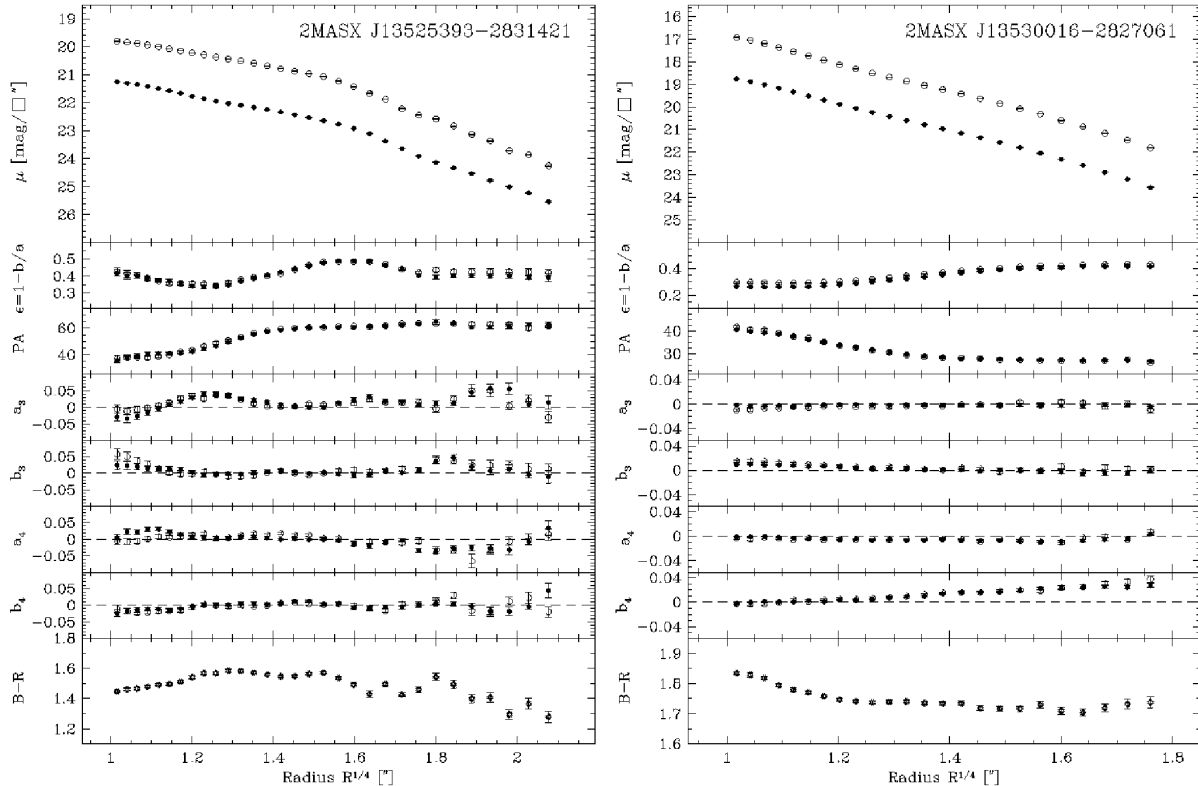


Figure 5. As in Figure 4.

Table 4. Photometric results

object (1)	B_T (2)	M_B (3)	R_T (4)	M_R (5)	$r_e(B)$ (6)	$r_e(R)$ (7)	$\mu_e(B)$ (8)	$\mu_e(R)$ (9)	$\mu_0(B)$ (10)	$\mu_0(R)$ (11)	n (12)
NGC 5328	12.31	-21.85	10.52	-23.64	53.16	58.31	24.00	22.46	15.17	12.87	4.23
NGC 5330	14.52	-19.64	12.77	-21.39	9.08	9.65	22.44	20.88	15.92	13.72	3.16
2MASX J13524838-2829584	15.48	-18.68	13.84	-20.32	5.94	5.90	21.80	20.18	17.51	15.71	2.14
2MASX J13523852-2830444	16.91	-17.25	15.10	-19.06							
bulge comp.	18.02	-16.14	17.73	-16.43	5.08	2.52	23.53	21.46	20.84	18.80	1.40
2MASX J13525393-2831421	16.88	-17.28	15.33	-18.83	6.74	6.92	23.39	21.64	21.05	19.28	1.24
MCG -5-33-29	14.69	-19.47	13.05	-21.11							
bulge comp.	17.04	-17.12	15.55	-18.61	1.32	1.61	20.13	18.94	18.31	17.83	1.00
2MASX J13530016-2827061	15.60	-18.56	13.87	-20.29							
bulge comp.	16.13	-18.03	15.11	-19.05	4.8	6.39	21.68	21.16	19.27	20.05	1.27

¹ group member galaxy identification; ² apparent total magnitude m_B ; ³ absolute total magnitude M_B ; ⁴ apparent total magnitude m_R ; ⁵ absolute total magnitude M_R ; ⁶ effective radius $r_e(B)$ [arcseconds]; ⁷ effective radius $r_e(R)$ [arcseconds]; ⁸ surface brightness $\mu_e(B)$ measured at the effective radius; ⁹ surface brightness $\mu_e(R)$; ¹⁰ central surface brightness $\mu_0(B)$; ¹¹ central surface brightness $\mu_0(R)$; ¹² Sérsic index n .

one relation, while the solid line marks the shift to apply for the transformation into the Lick system. Within the above set of working hypotheses, we derive the final corrected line strength indices for two radii, $r_e/8$ and $r_e/4$, for the four group galaxy members.

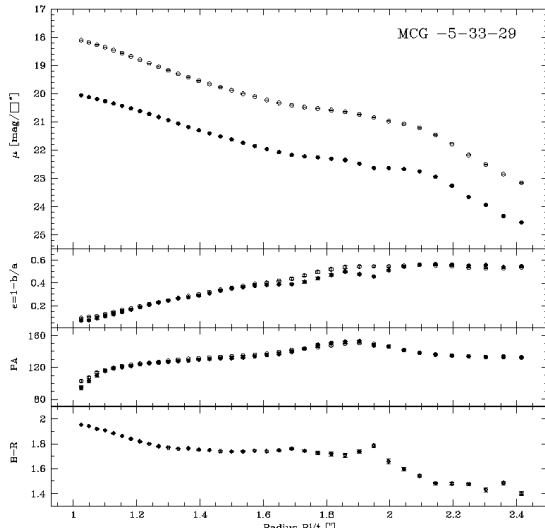
The correction of hydrogen absorption lines for emission infilling deserves a special comment. In particular, the measure of the $H\beta$ index of the underlying stellar population could be contaminated by a significant infilling due to the $H\beta$ emission component. We used the same template galaxy (NGC 1426) adopted in Rampazzo et al. (2005) to derive the $[OIII](\lambda 5007\text{\AA})$ emission EW for the member galaxies

and applied the correction $EW(H\beta_{em})/EW([OIII])=0.7$ proposed by Gonzalez (1993). Of the four galaxies shown in Figure 10 the only correction worth to mention is that applied to NGC 5330. The $H\beta$ indices for $r_e/8$ and $r_e/4$ move from 1.20 to 1.33 and 1.40 to 1.44 respectively after correction for emission infilling.

In order to characterize the underlying stellar population of the galaxies we have compared the fully corrected line-strength indices with Simple Stellar Population (SSPs) for a wide range of metallicities ($0.0004 < Z < 0.05$), ages ($1\text{Gyr} < t < 15\text{Gyr}$) and α -element enhancements ($0 < [\alpha/Fe] < 0.4$). For a full description of the mod-

Table 5. Neighbour galaxies within 1 Mpc

object	α (J2000.0)	δ (J2000.0)	type	m_B [mag]	cz [km s $^{-1}$]	D^1 [kpc]	Notes 2
2MASX J13521914-2839141	13 h 52 m 19.2 s	-28 $^{\circ}$ 39'14"	S0	16.7	4669 \pm 59	225	
2MASX J13514833-2823306	13 h 51 m 48.3 s	-28 $^{\circ}$ 23'31"	S0	16.6	4970 \pm 120	308	
2MASX J13530584-2847581	13 h 53 m 05.8 s	-28 $^{\circ}$ 47'58"	S0	15.2	5148	308	
2MASX J13514400-2814526	13 h 51 m 44.0 s	-28 $^{\circ}$ 14'52"	S0	16.1	5083 \pm 76	418	
2MASX J13513401-2841297	13 h 51 m 34.0 s	-28 $^{\circ}$ 41'30"	Sp	16.4	4407	420	
6dF J1354457-285159	13 h 54 m 45.6 s	-28 $^{\circ}$ 51'58"	Sp	16.2	4645 \pm 52	662	
2MASX J13531650-2900001	13 h 53 m 16.5 s	-29 $^{\circ}$ 00'00"	Sp	16.7	4689 \pm 45	697	
ESO 445 - G 64	13 h 52 m 21.0 s	-27 $^{\circ}$ 53'39"	SB(l)0/a	14.57	4907 \pm 40	720	
ESO 445 - G 51	13 h 49 m 20.9 s	-28 $^{\circ}$ 12'04"	(R)SAB(r)ab	14.56	5000 \pm 10	959	G
2MASX J13534359-2918241	13 h 53 m 43.6 s	-29 $^{\circ}$ 18'24"	S	15.70	4998 \pm 38	1009	

¹ Projected distance from NGC 5328; ² G – Group member of LGG 357 according to Garcia (1993).**Figure 6.** As in Figure 4.

els we refer to Annibali et al. (2005) and Annibali (2005). The solar-scaled composition SSPs have been derived according to the procedure described in Bressan et al. (1996) and on the index passbands definition of Worthey et al. (1994) and Worthey & Ottaviani (1997). The solar-scaled composition SSPs have been derived according to the procedure described in Bressan et al. (1996), while α -enhanced models are based on the Tripicco & Bell (1995), response functions and on new responses derived by model atmospheres and synthetic stellar spectra computed with the code ATLAS9 (Kurucz 1993). In the left and mid panels of Figure 10 we show respectively the classic $H\beta$ vs. $[\text{MgFe}]$ plane and the Mgb vs. $[\text{MgFe}]$ plane where we plot the measured galaxy indices for the apertures $r_e/8$ (full symbols) and $r_e/4$ (open symbols) together with model SSPs for different ages ($2\text{Gyr} < t < 15\text{Gyr}$), metallicities ($0.008 < Z < 0.05$) and enhancements ($[\alpha/\text{Fe}] = 0$, solid-dashed lines; $[\alpha/\text{Fe}] = 0.4$, dotted lines). The Seyfert MCG-5-33-29 and the S0s 2MASX J13523852-2830444 and 2MASX J13525393-2831421 are not included in the analysis since these galaxies have strong emission lines and the quality of

our spectra does not allow to recover a reliable value of the $H\beta$ absorption index.

The $H\beta$ vs. $[\text{MgFe}]$ plane, where models of constant age (solid lines) and constant metallicity (dashed lines) run almost orthogonally, is usually considered a powerful tool to disentangle age and total metallicity (see e.g. Worthey (1994), Worthey & Ottaviani (1997)). In this plane the α -elements enhancement has only a small effect on the SSPs: the $[\alpha/\text{Fe}] = 0.4$ models, represented by the dotted line, preserve the same $[\text{MgFe}]$ values and are only slightly shifted toward stronger $H\beta$. On the other hand, the effect of non-solar partitions is well visible in the Mgb vs. $[\text{MgFe}]$ plane. For a fixed element composition, lines of constant age and metallicity are basically degenerate and run almost parallel, while changes in the $[\alpha/\text{Fe}]$ ratio produce a considerable shift on the models.

From the combined analysis of the two planes the following considerations can be done: NGC 5328, NGC 5330 and 2MASX J13530016-2827061 have quite old stellar populations, super-solar metallicities and super-solar $[\alpha/\text{Fe}]$ ratios. 2MASX J13524838-2829584 presents a super-solar metallicity as well, but no α -enhancement. The strong $H\beta$ value however suggests the occurrence of a recent burst of star formation. We are pretty well confident about this result because the galaxy is not affected by emission and the $H\beta$ index is therefore reliable. For what concerns the large error on the measured velocity dispersion, it mainly affects the velocity dispersion correction for the $[\text{MgFe}]$ and Mgb indices, but has almost no effect on the $H\beta$. This translates into a larger uncertainty in the derived metallicity than in the derived age, which is always < 4 Gyr.

In order to derive SSP parameters (age, Z and $[\alpha/\text{Fe}]$) we have devised a simple but robust algorithm based on the Mgb , $< \text{Fe} >$ and $H\beta$ indices (Annibali (2005)). For each galaxy the best-fit age, Z and $[\alpha/\text{Fe}]$ are derived by searching in a finely spaced grid of points in the ($H\beta$, Mgb and $< \text{Fe} >$) space the SSP model that matches the observed indices. In Fig. 10 (right panel) the derived SSP parameters with the associated errors are plotted as a function of central velocity dispersion for the galaxies NGC 5328, NGC 5330, 2MASX J13530016-2827061 and 2MASX J13524838-2829584. The dotted and solid lines represent the best fit for the low and high density environments obtained as function of the velocity dispersion by

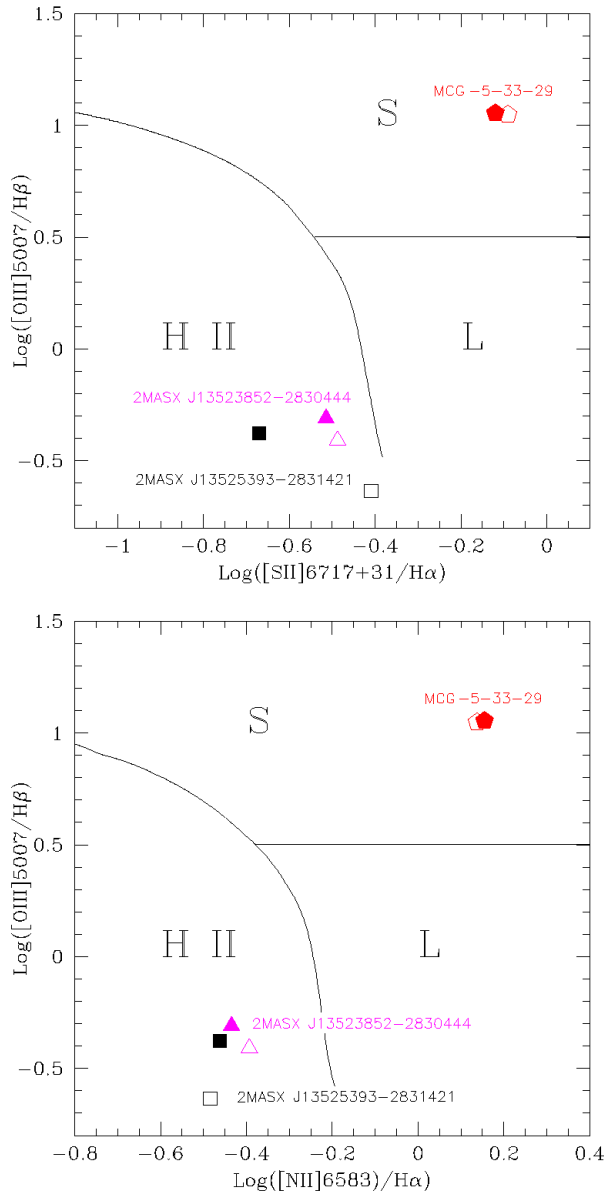


Figure 8. Diagnostic diagrams for emission-line galaxies: logarithmic line ratios of $[S\text{ II}]\lambda 6617 + 31/\text{H}\alpha$ vs. $[O\text{ III}]\lambda 5007/\text{H}\beta$ (top panel) and $[N\text{ II}]\lambda 6583/\text{H}\alpha$ vs. $[O\text{ III}]\lambda 5007/\text{H}\beta$ (bottom panel). The emission-line flux was extracted within an aperture with radius $R_e/8$ (open symbols) and $R_e/4$ (full symbols). The bold line separates H II region like objects from AGNs.

Thomas et al. (2005). In the $[\alpha/\text{Fe}]$ vs. $\log \sigma$ plot the two environments share the same best fit relation. Both the trend and the dispersion of our values are similar to those found in the set of object studied in low and high density environments by Thomas et al. (2005).

5 DISCUSSION AND CONCLUSIONS

We analyzed photometric and spectroscopic properties of seven galaxies members of the NGC 5328 group of galaxies. We analyzed the galaxy structure, studied the emission line properties and attempted to infer the star formation his-

tory of the galaxies in the group from the comparison of the measured line-strength indices with SSP models.

The NGC 5328 group represents a relatively compact structure of galaxies lying in the outskirts of a galaxy cluster: It consists of seven galaxies aligned in a chain spanning about 200 kpc. The group has the same redshift of Abell 3574 which has a projected distance of 2.4 Mpc. It appears thus particularly suited to investigate processes occurring in galaxy groups which are likely to be accreted by galaxy clusters. A set of 10 neighbour galaxies with known redshift within 1 Mpc (see Table 5) has been extracted from NED. These objects do not show a symmetrical projected distribution around the group, their redshift distribution is plotted (together with the confirmed group members) in Figure 11 (bottom panel). We notice a sort of morphology segregation in the NGC 5328 group: two ellipticals are forming the center of the group (in projection and in redshift space) while the lenticulars are located from small to medium distances, the spiral MCG -5-33-29 has the largest projected separation from NGC 5328. No elliptical galaxies are found in the outskirts of the group: the neighbour galaxies in Table 5 are faint spiral or lenticular galaxies. In the field covered by our images we investigated the presence of a dwarf galaxy population. Figure 11 displays the R-band magnitude distribution for the sample of candidate dwarfs and the colour-magnitude relation of the Coma cluster (Secker et al. 1997) superposed to our data. Since this relation perfectly fits our data, the same colour restriction for probable dwarf galaxy group members of $0.7 \leq (B-R) \leq 1.9$, representing generous limits to the early-type sequence, was applied to our sample. For the Coma cluster, these limits were found to remove the vast majority of background objects. The resulting sample of likely dwarf galaxy group members consisting of 68 objects with a mean colour of $(B-R) = 1.32 \pm 0.28$ magnitudes is given in the Appendix, Tables A1 and A2.

The presence of a large number of dwarf galaxies in poor groups is also suggested by Khosroshahi et al. (2004, and references therein) looking for differences in the galaxy population of X-ray dim and X-ray bright nearby groups. The photometric characteristic of the groups can be easily shown using the Hamabe-Kormendy relation, a photometric projection of the fundamental plane connecting the effective radius R_e with the surface brightness at this radius μ_e . This relation can be used to divide early-type galaxies in ordinary and bright families (Hamabe & Kormendy 1987; Capaccioli et al. 1992). Bright elliptical galaxies follow the relatively tight relation of $\mu_e = 2.94 \log R_e + 20.75$ while the ordinary objects are spread over the region below this relation with a borderline at $R_e = 3$ kpc. This ordinary class is believed to participate in the formation of the bright ellipticals following the HK relation via successive merging episodes, although the recent simulations of Evstigneeva et al. (2004) suggest that only progenitors of higher surface brightness from the ordinary object class can produce an outcome lying on the HK relation. Figure 12 shows the Hamabe-Kormendy relation for galaxies of the NGC 5328 group together with data obtained in paper I and II for different small-scale systems of galaxies compared with the galaxy group sample studied by Khosroshahi et al. (2004). Most of the early-type galaxies in groups are ordinary objects, while NGC 5328 is located in the region of

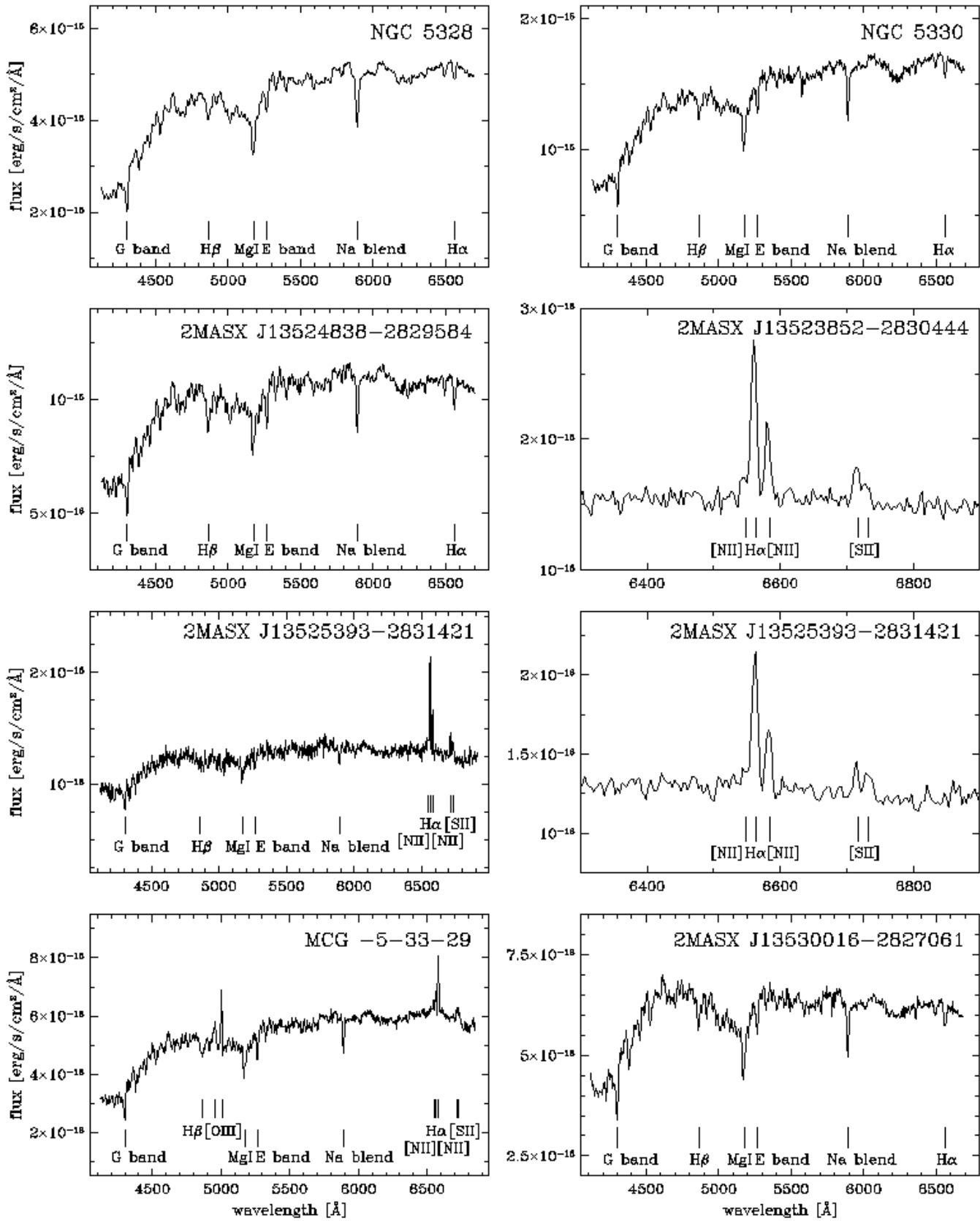


Figure 7. Spectra of the NCG 5328 group member galaxies.

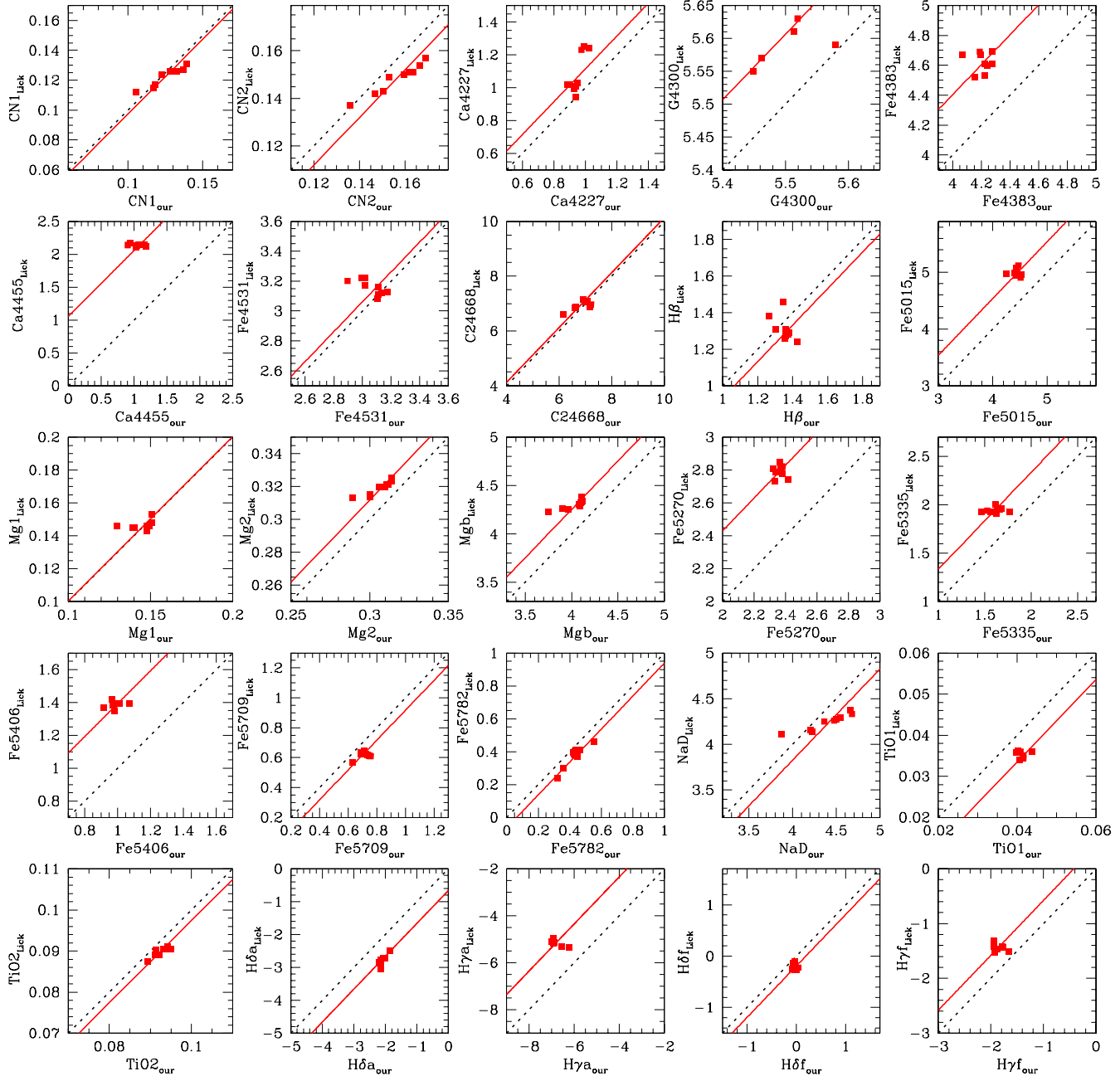


Figure 9. Comparison of passband measurements from our spectra of NGC 5328 and Lick calibrated apertures for the same galaxy in Rampazzo et al. (2005). The dotted line is the one to one relation while the solid line is the *robust straight-line fit* to the filled squares (see text and Rampazzo et al. (2005)).

bright galaxies, suggesting an advanced stage in its evolution.

Signatures of past and/or recent interactions between the group members have been investigated looking for fine structures in the galaxies and analyzing their line-strength indices. Only minor fine structures have been detected: a faint ripple is found in NGC 5330, however, no recent star formation episodes are suggested for this galaxy by the $H\beta$ vs. MgFe line-strength indices. The extremely boxy isophotes of 2MASX J13524838-2829584 are believed to be

connected to a merging event (e.g. Schweizer 1996). Line strength indices suggest that this object may have experienced a recent star formation episode. A warped disc component emerges from the model subtracted image of 2MASX J13530016-2827061. Since Nelson & Tremaine (1995) conclude that warps cannot be primordial structures but must have either a recent or a continuous excitation mechanism, we suggest an ongoing interaction of this galaxy with nearby group members.

Star formation and nuclear activity seem present only

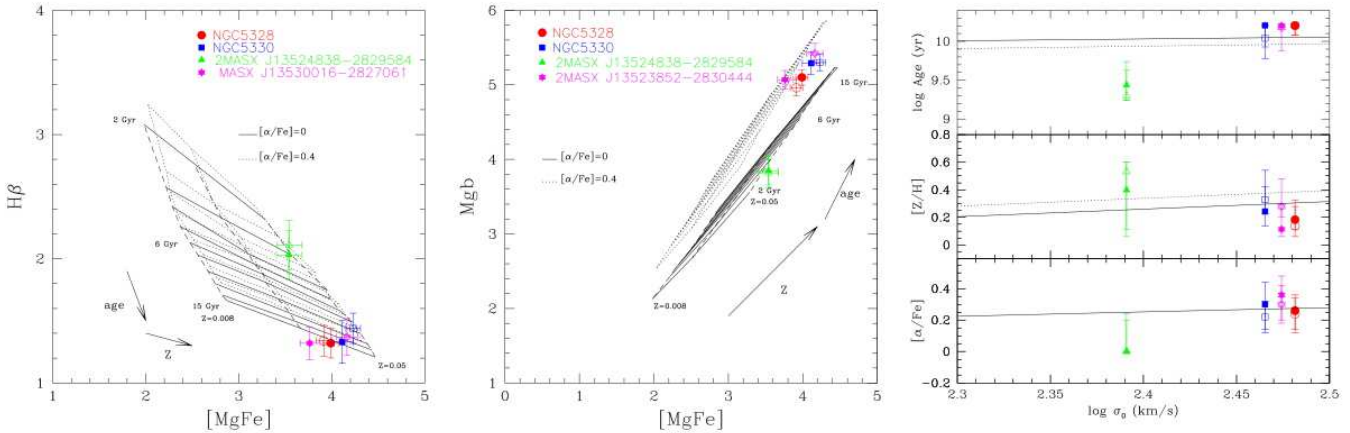


Figure 10. **left panel:** $H\beta$ vs. $[MgFe]$ plane where we plot the measured indices for two apertures ($R_e/8$, solid symbols, and $R_e/4$, open symbols) for those galaxies with no emission lines, together with SSP models with $0.008 < Z < 0.05$, $2 \text{ Gyr} < t < 15 \text{ Gyr}$ and $[\alpha/Fe] = 0$ and 0.4. Solid “horizontal” lines indicate solar-scaled models of constant age, while “vertical” dashed lines are models of constant metallicity. Dotted lines represent α -enhanced SSPs. **(mid panel):** Mgb vs. $MgFe$ plane. Lines of constant age and metallicity are degenerate and run almost parallel. The effect of α -enhancement is instead well separated in this plane. **(right panel)** From top to bottom we plot the derived ages, metallicities and $[\alpha/Fe]$ ratios for the NGC 5328 group galaxy members which do not show strong emission lines, namely NGC 5328, NGC 5330, 2MASX J13530016-2827061 and 2MASX J13524838-2829584. Different symbols refer to different objects and apertures with the same meaning as in the previous panels. The dotted and solid lines represent the best fit for the low and high density environments obtained as function of the velocity dispersion by Thomas et al. (2005). In the $[\alpha/Fe]$ vs. $\log \sigma$ plot the two environments share the same best fit relation.

in the projected outskirts of the group. Spectral signatures of star formation are present in the galaxies 2MASX J13523852-2830444 and 2MASX J13525393-2831421. Nuclear activity is present in MCG -5-33-29: the strong forbidden lines of [O III] and [N II] ratios indicate a type 2 Seyfert activity.

Recent results (Proctor et al. 2004; Mendes de Oliveira et al. 2005) suggest that galaxies in Hickson compact group (HCG) are generally old, a result that contradicts the expectations from various scenarios for compact group formation. In particular, Diaferio et al. (1994) and Governato et al. (1996) suggest that a large fraction of ellipticals in compact groups should have a merging origin and then should consequently appear to be young which is at odd with above observations. NGC 5328 has not the characteristics of a compact group but its has some similarity with them. In particular, the present study shows that this group is composed of a large fraction of early-type members, as HCG (Hickson et al. 1988). Furthermore, the dominant “bona fide” elliptical NGC 5328 and the bright companion NGC 5330 have a quite old stellar population and less luminous nearby early-type companions show both, signatures of recent and ongoing star formation. We may depict NGC 5328 as an *evolving group* with a plethora of possibly associated dwarf galaxies, which could be among the drivers of the main galaxy evolution.

Most of the NGC 5328 group features are shared with poor groups with X-ray diffuse emission (see e.g. Mulchaey 2000). RASS reveals that NGC 5328 is a relatively strong X-ray emitter (Beuing et al. 1999): new X-ray observations would clarify the nature and the characteristics of the emission (e.g. the presence of a “group” component in the hot diffuse medium (Mulchaey 2000) yielding valuable clues about the evolutionary phase of this group.

ACKNOWLEDGMENTS

RG and WWZ acknowledge the support of the Austrian Science Fund (project P14783). RG, RR and WWZ acknowledge the support of the Austrian and Italian Foreign Offices in the framework science and technology bilateral collaboration (project number 25/2004) This research has made use of the NASA/IPAC Extragalactic Database (NED) which is operated by the Jet Propulsion Laboratory, California Institute of Technology, under contract to the National Aeronautics and Space Administration. The Digitized Sky Survey (DSS) was produced at the Space Telescope Science Institute under U.S. Government grant NAG W-2166. The images of these surveys are based on photographic data obtained using the Oschin Schmidt Telescope on Palomar Mountain and the UK Schmidt Telescope. The plates were processed into the present compressed digital form with the permission of these institutions.

REFERENCES

- Annibali F., Rampazzo R., Bressan A., Danese L., Bertone E., Chavez M., Zeilinger, W.W., 2005, in Dettmar R.-J., Klein U., Salucci P., eds, Proc. Baryons in Dark Matter Halos, PoS, SISSA, in press (astro-ph/0501302)
- Annibali F., 2005, Ph.D. thesis, SISSA, in preparation
- Bower R.G., Balogh M.L., 2004, in Mulchaey J.S., Dressler A., Oemler A., eds, Proc. Clusters of Galaxies: Probes of Cosmological Structure and Galaxy Evolution, Cambridge University Press, p. 326
- Bertin E., Arnouts S., 1996, A&AS, 117, 393
- Beuing J., Döbereiner S., Böhringer H., Bender R., 1999, MNRAS, 302, 209
- Bressan A., Chiosi C., Tantalo R., 1996, A&A, 311, 425
- Buta R., 1995, ApJS, 96, 39

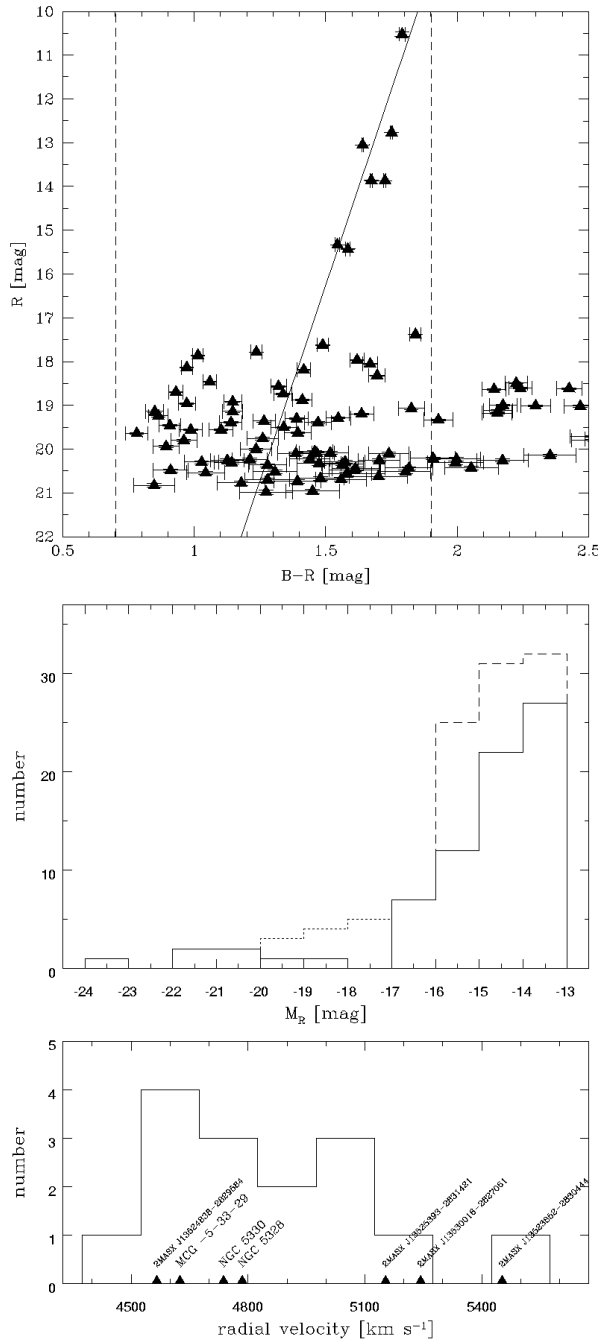


Figure 11. (upper panel) Colour-magnitude relation for the group including bright galaxies at the top and the candidate dwarf galaxies in the field of the group. Dwarf galaxy candidates are enclosed within the dashed lines, the solid line represents the colour-magnitude relation for the Coma cluster (see text). The list of the objects is given in Appendix A. (mid panel) Absolute R magnitude distribution within the group including all extended objects (long dashed line), dwarf member candidates after applying the colour restriction (solid line) and neighbour galaxies within 1 Mpc (dotted line). (bottom panel) Redshift distribution of known group members, including those detected in this paper, and of neighbour galaxies within 1 Mpc.

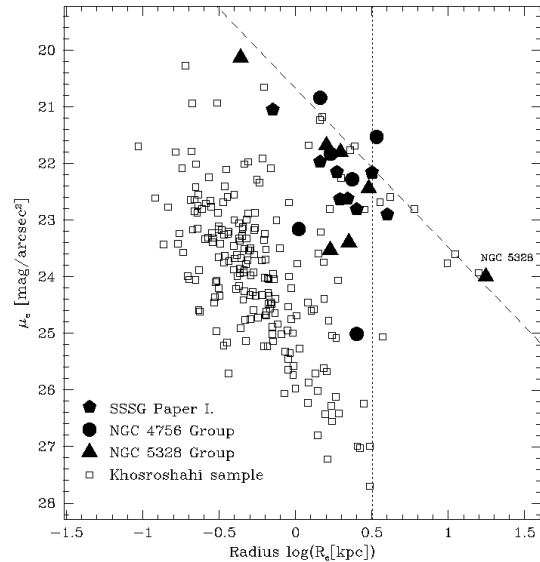


Figure 12. Effective radius (in kiloparsec) vs. the effective B surface brightness. The diagonal long-dashed line marks the HK87 relation followed by elliptical galaxies and early-type bulges. The vertical dotted line at $\log R_e = 0.5$, i.e., 3 kpc ($H_0 = 70 \text{ km s}^{-1} \text{ Mpc}^{-1}$) separates bright from ordinary ellipticals according to Capaccioli et al. (1992). The plot shows the present data (triangles) overplotted to measurements obtained in paper I and paper II (pentagons). Open squares are from the groups studied by Khosroshahi et al. (2004) who used a similar procedure selecting dwarf galaxy candidates by means of the R-(B-R) colour-magnitude relation.

Capaccioli M., Caon N., D'Onofrio M., 1992, in Danziger I.J., Zeilinger W.W., Kjær, K., eds, Proc. Structure, Dynamics and Chemical Evolution of Early-Type Galaxies, ESO, Garching, p. 43
 Coziol R., Iovino A., de Carvalho R.R., 2000, AJ, 120, 47
 de Carvalho R.R., da Costa L.N., 1988, ApJS, 68, 173
 de Vaucouleurs G., de Vaucouleurs A., Corwin H.G. Jr., Buta R.J., Paturel G., Fouqué P., 1991, Third Reference Catalog of Bright Galaxies, Springer, New York
 Diaferio A., Geller M.J., Ramella M., 1994, AJ, 107, 868
 Duc P.-A., Bournaud F., Masset F., 2004, A&A, 427, 803.
 Evstigneeva E.A., de Carvalho R.R., Ribeiro A.L., Capelato H.V., 2004, astro-ph/0410143
 Garcia A.M., 1993, A&AS, 100, 47
 Gill S.P.D., Knebe A., Gibson B.K., 2005, MNRAS, 356, 1327
 Giuricin G., Marinoni C., Ceriani L., Pisani A., 2000, ApJ, 543, 178
 Gomez P.L., et al., 1993, MNRAS, 584, 210
 Gonzalez J.J., 1993, Ph.D. Thesis, Univ. California, Santa Cruz
 Governato F., Tozzi P., Cavaliere, A. 1996, ApJ, 458, 18
 Grützbauch R., Kelm B., Focardi P., Rampazzo R., Zeilinger, W.W., 2005, AJ, 129, 1832
 Hamabe M., Kormendy J., 1987, in de Zeeuw T., ed, Proc. IAU Symp. 127, Structure and Dynamics of elliptical Galaxies, Reidel, Dordrecht, p. 379 (HK87)
 Heisler J., Tremaine S., Bahcall J.N., 1985, ApJ, 298, 8
 Henriksen M., Cousineau S., 1999, ApJ, 511, 595

Hickson P., Kindl E., Huchra J. 1988, *ApJ*, 331, 64

Jedrzejewski R., 1987, *MNRAS*, 226, 747

Jones C., Forman W., 1999, *ApJ*, 511, 65

Jones L.R., Ponman T.J., Horton A., Babul A., Ebeling H., Burke D., 2003, *MNRAS*, 434, 627

Kelm B., Focardi P., 2004, *A&A*, 418, 937

Kelm B., Focardi P., Zitelli V., 2004, *A&A*, 418, 25

Kennicutt R.C., Schweizer F., Barnes J., 1996, Galaxies: Interactions and Induced Star Formation, Saas-Fee Advanced Course 26

Khosroshahi H.G. Raychaudhury S., Ponman T.J., Miles T.A., Forbes D.A., 2004, *MNRAS*, 349, 527

Klemola A.R., 1969, *AJ*, 74, 804

Kurucz R.L., 1993, ATLAS9 Stellar Atmosphere Programs and 2 km s⁻¹ grid, (Kurucz CD-ROM No. 13)

Lewis I., et al., 2002, *MNRAS*, 334, 673

Mahdavi A., Geller M. J., 2001, *ApJ*, 554, 129

Maia M.A.G.; Machado R.S., Willmer C.N.A., 2003, *AJ*, 126, 1750

Mendes de Oliveira C., Coehlo P., González J.J., Barbay B. 2005, *AJ*, 130, 55

Meza A., Navarro J.F., Steinmetz M., Eke V.R., 2003, *ApJ*, 590, 619

Mihos C.J., 2004, in Mulchaey J.S., Dressler A., Oemler A., eds, Proc. Clusters of Galaxies: Probes of Cosmological Structure and Galaxy Evolution, Cambridge University Press, p. 278

Miles T.A., Raychaudhury S., Forbes D.A., Goudfrooij P., Ponman T.J., Kozhurina-Platais V., 2004, *MNRAS*, 355, 785

Moore B., Katz N., Lake G., Dressler A., Oemler A. Jr., 1996, *Nature*, 379, 613

Mulchaey J.S., 2000, *ARA&A*, 38, 289

Mulchaey J.S., Davis D.S., Mushotzky R.F., Burstein D., 1993, *ApJ*, 404, L9

Mulchaey, J. S., Davis D.S., Mushotzky R.F., Burstein D., 1996, *ApJ*, 456, 80

Mulchaey J.S., Zabludoff A.I., 1999, *ApJ*, 514, 133

Mulchaey J.S., Davis D.S., Mushotzky R.F., Burstein D., 2003, *ApJS*, 145, 39

Nelson R.W., Tremaine S., 1995, *MNRAS*, 275, 897

Peng C.Y., Ho L.C., Impey C.D., Rix H., 2002, *AJ*, 124, 266

Ponman T.J., Bourner P.D.J., Ebeling H., Böhringer H., 1996, *MNRAS*, 283, 690

Proctor R.N., Forbes D.A., Hau G.K.T., Beasley M.A., De Silva G.M. et al. 2004, *MNRAS*, 349, 1381

Puzia, T.H., Saglia, R.P., Kissler-Patig, M., Maraston, C., Greggio, L. et al. 2002, *A&A*, 395, 45

Rampazzo R., Covino S., Trinchieri G., Reduzzi L., 1998, *A&A*, 330, 423

Rampazzo R., Annibali F., Bressan A., Longhetti M., Padoa F., Zeilinger W.W., 2005, *A&A*, 433, 497

Richter O.-G., 1984, *A&AS*, 58, 131

Rines K., Gelle, M.J., Kurtz M.J., Diaferio A., 2003, *AJ*, 126, 2152

Schweizer F., 1996, Galaxies: Interactions and Induced Star Formation, Saas-Fee Advanced Course 26, 105

Secker J., Harris W.E., Plummer J.D., 1997, *PASP*, 109, 1377

Smith R.J., Lucey J.R., Hudson M.J., Schlegel D.J., Davies R.L., 2000, *MNRAS*, 313, 469

Struble M.F., Rood H.J., 1999, *ApJS*, 125, 35

Tanvua L., Kelm B., Focardi P., Rampazzo R., Zeilinger W.W., 2003, *AJ*, 126, 1245

Thomas D., Maraston C., Bender R., de Oliveira C.M., 2005, *ApJ*, 621, 674

Trager S.C., Worthey G., Faber S.M., Burstein D., Gonzalez J.J., 1998, *ApJS*, 116, 1

Trinchieri G., Rampazzo R., 2001, *A&A*, 374, 454

Trippicco M.J., Bell R.A., 1995, *AJ*, 110, 3035

Veilleux S., Osterbrock D.E., 1987, *ApJS* 63, 295

Verdes-Montenegro L., Yun M.S., Perea J., del Olmo A., Ho P.T.P., 1998, *ApJ* 498, 89

Worthey G., 1994, *ApJS*, 95, 107

Worthey G., Faber S.M., Gonzalez J.J., Burstein D., 1994, *ApJS*, 94, 687

Worthey G., Ottaviani D.L., 1997, *ApJS*, 111, 377

APPENDIX A: TABLES OF FAINT GROUP MEMBER CANDIDATES

Table A1. Faint group member candidates

object ¹	α (J2000.0)	δ (J2000.0)	m_R [mag]	M_R [mag]	(B-R) [mag]
767	13 53 14.045	-28 25 49.178	17.380 \pm 0.008	-16.78	1.841 \pm 0.022
343	13 53 02.685	-28 30 16.420	17.617 \pm 0.012	-16.55	1.488 \pm 0.022
1105	13 53 07.950	-28 27 53.585	17.785 \pm 0.010	-16.38	1.236 \pm 0.021
462	13 52 47.719	-28 30 04.422	17.856 \pm 0.010	-16.31	1.014 \pm 0.020
1203	13 53 14.474	-28 28 48.712	17.966 \pm 0.011	-16.20	1.619 \pm 0.026
680	13 52 49.206	-28 28 46.751	18.055 \pm 0.012	-16.11	1.669 \pm 0.029
749	13 53 11.407	-28 25 05.067	18.137 \pm 0.011	-16.03	0.971 \pm 0.022
159	13 52 36.845	-28 32 28.946	18.189 \pm 0.012	-15.97	1.416 \pm 0.027
1007	13 52 56.378	-28 27 02.921	18.318 \pm 0.013	-15.84	1.695 \pm 0.032
86	13 52 39.197	-28 32 59.800	18.439 \pm 0.013	-15.72	2.97 \pm 0.057
634	13 52 58.040	-28 29 03.726	18.461 \pm 0.014	-15.70	1.059 \pm 0.027
492	13 52 57.540	-28 29 51.576	18.495 \pm 0.014	-15.67	2.224 \pm 0.042
712	13 53 13.512	-28 28 19.031	18.507 \pm 0.014	-15.66	2.643 \pm 0.051
676	13 53 13.445	-28 28 46.790	18.569 \pm 0.014	-15.59	1.32 \pm 0.030
784	13 53 05.695	-28 25 11.204	18.588 \pm 0.014	-15.57	2.669 \pm 0.054
724	13 53 02.792	-28 27 19.298	18.604 \pm 0.014	-15.56	2.24 \pm 0.045
667	13 53 13.213	-28 28 44.546	18.620 \pm 0.015	-15.54	2.425 \pm 0.048
1147	13 52 55.937	-28 26 56.279	18.636 \pm 0.016	-15.53	2.14 \pm 0.046
717	13 53 10.249	-28 24 49.202	18.698 \pm 0.015	-15.46	0.93 \pm 0.028
564	13 52 57.758	-28 28 52.981	18.722 \pm 0.016	-15.44	3.067 \pm 0.071
1022	13 53 08.451	-28 26 49.969	18.735 \pm 0.016	-15.43	1.337 \pm 0.034
274	13 52 38.762	-28 31 39.396	18.876 \pm 0.017	-15.29	1.411 \pm 0.037
43	13 52 38.772	-28 33 34.629	18.916 \pm 0.017	-15.25	1.146 \pm 0.034
373	13 53 01.384	-28 30 45.466	18.936 \pm 0.018	-15.23	2.736 \pm 0.066
10	13 52 52.445	-28 33 56.620	18.960 \pm 0.017	-15.20	0.971 \pm 0.033
93	13 52 50.584	-28 33 07.252	18.998 \pm 0.018	-15.16	2.174 \pm 0.053
831	13 53 05.104	-28 25 43.464	19.011 \pm 0.018	-15.15	2.298 \pm 0.056
1148	13 52 45.610	-28 27 01.086	19.020 \pm 0.024	-15.14	2.468 \pm 0.063
890	13 53 00.848	-28 26 01.148	19.073 \pm 0.021	-15.09	1.825 \pm 0.050
1140	13 52 47.173	-28 28 21.117	19.121 \pm 0.021	-15.04	2.155 \pm 0.057
533	13 53 14.715	-28 28 36.039	19.140 \pm 0.019	-15.02	0.849 \pm 0.035
584	13 53 07.866	-28 28 56.519	19.141 \pm 0.020	-15.02	1.146 \pm 0.039
835	13 53 04.508	-28 25 41.366	19.179 \pm 0.019	-14.98	2.152 \pm 0.057
523	13 52 57.716	-28 28 32.220	19.198 \pm 0.020	-14.96	1.636 \pm 0.047
416	13 52 42.450	-28 30 23.788	19.206 \pm 0.022	-14.96	2.702 \pm 0.076
903	13 53 03.593	-28 25 59.642	19.242 \pm 0.020	-14.92	0.863 \pm 0.036
833	13 53 13.943	-28 27 44.427	19.291 \pm 0.020	-14.87	1.547 \pm 0.047
660	13 52 46.516	-28 29 35.698	19.306 \pm 0.021	-14.86	1.389 \pm 0.045
710	13 53 04.732	-28 24 37.850	19.334 \pm 0.021	-14.83	1.928 \pm 0.056
765	13 53 16.571	-28 24 54.930	19.356 \pm 0.021	-14.81	2.958 \pm 0.089
886	13 53 09.681	-28 26 08.411	19.362 \pm 0.021	-14.80	1.265 \pm 0.043
893	13 53 10.600	-28 25 37.048	19.392 \pm 0.022	-14.77	1.139 \pm 0.043
144	13 52 43.840	-28 32 41.331	19.395 \pm 0.027	-14.77	1.47 \pm 0.052
339	13 52 56.643	-28 31 06.975	19.419 \pm 0.022	-14.74	2.713 \pm 0.082
443	13 52 56.447	-28 30 18.392	19.459 \pm 0.022	-14.70	0.907 \pm 0.040
228	13 52 48.345	-28 31 59.775	19.504 \pm 0.023	-14.66	1.34 \pm 0.049
735	13 53 00.874	-28 24 52.194	19.557 \pm 0.024	-14.61	0.986 \pm 0.044
594	13 52 49.465	-28 29 07.259	19.558 \pm 0.025	-14.60	1.102 \pm 0.046
828	13 53 07.375	-28 25 31.949	19.625 \pm 0.024	-14.54	1.394 \pm 0.052
1065	13 52 44.363	-28 27 27.749	19.641 \pm 0.024	-14.52	0.781 \pm 0.042
933	13 53 10.738	-28 26 30.416	19.711 \pm 0.026	-14.45	2.514 \pm 0.087
874	13 53 03.736	-28 25 30.935	19.759 \pm 0.034	-14.40	1.26 \pm 0.059
901	13 53 03.161	-28 26 12.292	19.776 \pm 0.035	-14.39	2.577 \pm 0.092
328	13 52 44.171	-28 31 14.701	19.797 \pm 0.027	-14.37	2.523 \pm 0.090
982	13 53 16.312	-28 26 43.636	19.805 \pm 0.028	-14.36	0.96 \pm 0.050
298	13 52 41.097	-28 31 29.559	19.941 \pm 0.029	-14.22	0.893 \pm 0.051
1003	13 52 56.896	-28 27 24.871	20.003 \pm 0.031	-14.16	1.235 \pm 0.061

¹ SExtractor object identification

Table A2. Faint group member candidates. (cont.)

object ¹	α (J2000.0)	δ (J2000.0)	m_R [mag]	M_R [mag]	B - R [mag]
76	13 52 48.699	-28 33 16.953	20.058 \pm 0.035	-14.10	1.458 \pm 0.069
739	13 53 13.683	-28 25 00.555	20.087 \pm 0.034	-14.08	1.517 \pm 0.070
607	13 53 03.679	-28 29 12.862	20.091 \pm 0.031	-14.07	1.466 \pm 0.068
141	13 52 49.107	-28 32 46.192	20.101 \pm 0.036	-14.06	1.386 \pm 0.069
635	13 52 45.502	-28 27 07.050	20.102 \pm 0.035	-14.06	1.74 \pm 0.077
1174	13 52 54.039	-28 26 52.981	20.144 \pm 0.034	-14.02	2.353 \pm 0.100
822	13 53 02.007	-28 27 17.293	20.210 \pm 0.033	-13.95	1.908 \pm 0.086
1201	13 53 02.989	-28 28 48.253	20.228 \pm 0.040	-13.93	1.997 \pm 0.093
596	13 52 58.807	-28 29 09.795	20.230 \pm 0.041	-13.93	1.439 \pm 0.077
299	13 52 36.507	-28 31 31.002	20.238 \pm 0.034	-13.92	1.211 \pm 0.066
315	13 52 40.791	-28 31 22.086	20.258 \pm 0.035	-13.90	1.125 \pm 0.065
74	13 52 41.258	-28 33 22.562	20.258 \pm 0.034	-13.90	1.703 \pm 0.080
282	13 52 56.080	-28 31 37.776	20.258 \pm 0.034	-13.90	2.172 \pm 0.099
1114	13 52 46.274	-28 27 59.216	20.292 \pm 0.035	-13.87	1.573 \pm 0.077
802	13 52 59.374	-28 25 14.930	20.298 \pm 0.037	-13.86	1.028 \pm 0.065
754	13 52 59.190	-28 24 46.133	20.309 \pm 0.048	-13.85	1.993 \pm 0.106
867	13 53 06.404	-28 27 50.912	20.310 \pm 0.035	-13.85	1.142 \pm 0.067
918	13 53 16.367	-28 27 38.204	20.332 \pm 0.047	-13.83	1.474 \pm 0.084
1130	13 53 11.607	-28 28 12.106	20.340 \pm 0.037	-13.82	1.564 \pm 0.080
447	13 52 44.218	-28 30 19.272	20.366 \pm 0.037	-13.80	1.278 \pm 0.072
856	13 52 48.514	-28 27 41.771	20.430 \pm 0.041	-13.73	2.053 \pm 0.103
620	13 53 14.759	-28 29 17.774	20.435 \pm 0.036	-13.73	1.816 \pm 0.090
307	13 52 42.793	-28 31 26.273	20.452 \pm 0.042	-13.71	1.613 \pm 0.089
114	13 52 53.684	-28 32 55.839	20.480 \pm 0.048	-13.68	1.608 \pm 0.097
541	13 52 50.344	-28 28 40.114	20.486 \pm 0.038	-13.68	0.91 \pm 0.067
1023	13 52 46.371	-28 26 54.904	20.519 \pm 0.049	-13.64	1.307 \pm 0.084
421	13 52 51.490	-28 30 30.187	20.519 \pm 0.039	-13.64	1.803 \pm 0.094
1129	13 52 47.014	-28 28 10.742	20.540 \pm 0.039	-13.62	1.043 \pm 0.072
200	13 52 44.304	-28 31 58.908	20.564 \pm 0.046	-13.60	1.58 \pm 0.095
1030	13 53 10.184	-28 27 47.998	20.626 \pm 0.064	-13.54	1.7 \pm 0.111
464	13 53 03.242	-28 30 10.125	20.667 \pm 0.042	-13.50	1.48 \pm 0.089
919	13 53 15.473	-28 27 49.968	20.695 \pm 0.046	-13.47	1.558 \pm 0.098
1020	13 53 01.946	-28 27 10.920	20.700 \pm 0.045	-13.46	1.278 \pm 0.086
1187	13 53 11.477	-28 28 36.067	20.733 \pm 0.044	-13.43	1.392 \pm 0.090
1043	13 52 53.579	-28 27 17.626	20.774 \pm 0.054	-13.39	1.178 \pm 0.091
762	13 53 08.939	-28 27 47.274	20.828 \pm 0.047	-13.33	0.847 \pm 0.079
247	13 52 47.250	-28 31 52.194	20.963 \pm 0.054	-13.20	1.45 \pm 0.103
702	13 52 38.071	-28 29 44.466	20.981 \pm 0.056	-13.18	1.273 \pm 0.100

¹ SExtractor object identification